Available online at www.sciencedirect.com
SCIENCE DIRECT
Journal of Catalysis 235 (2005) 209–220
JOURNAL OF CATALYSIS
www.elsevier.com/locate/jcat

Photocatalytic oxidation of acetonitrile in gas–solid and liquid–solid regimes

Maurizio Addamo [a], Vincenzo Augugliaro [a], Salvatore Coluccia [b], Maria Giulia Faga [b,c], Elisa García-López [a], Vittorio Loddo [a], Giuseppe Marcì [a], Gianmario Martra [b], Leonardo Palmisano [a,*]

[a] *Dipartimento di Ingegneria Chimica dei Processi e dei Materiali, Università degli Studi di Palermo, Viale delle Scienze, 90128 Palermo and UdR Palermo 1 Interuniversity Consortium "Chemistry for the Environment" – INCA, Italy*
[b] *Dipartimento di Chimica IFM – NIS Center of Excellence, Università degli Studi di Torino, Via Pietro Giuria 7, 10125 Torino and UdR Torino 1 Interuniversity Consortium "Chemistry for the Environment" – INCA, Italy*
[c] *CNR – Istituto di Scienza e Tecnologia dei Materiali Ceramici, Strada delle Cacce 73, 10135 Torino, Italy*

Received 17 May 2005; revised 12 July 2005; accepted 7 August 2005

Abstract

Photocatalytic degradation of acetonitrile was carried out in both gas–solid and liquid–solid regimes using two commercial TiO_2 catalysts (Merck and Degussa P25). For the gas–solid regime, a continuous annular photoreactor was used. The influence on photodegradation kinetics of the gas flow rate and concentrations of acetonitrile, oxygen, and water was investigated. Acetonitrile degradation products detected in the gas phase included carbon dioxide and hydrogen cyanide. The same photoactivity was exhibited in the presence and in the absence of water vapour. The liquid–solid regime used a batch photoreactor with an immersed lamp (the same as for the gas–solid regime). The oxidation products detected in the solution were cyanide, cyanate, nitrite, nitrate, methanoate, and carbonate ions. The Langmuir–Hinshelwood kinetic model fit the photoreactivity data obtained in both regimes and allowed us to determine the rate constant and equilibrium adsorption constant values. The adsorption constant and kinetic constant value were lower in the liquid–solid regime than in the gas–solid regime. The Merck catalyst had higher values of these parameters for both regimes than the Degussa P25 catalyst. An evaluation of the possible competition between acetonitrile and water molecules for the surface sites of the photocatalyst (Ti^{4+} ions and hydroxyl groups) revealed that for high H_2O/CH_3CN ratios, as is typical for the photo-oxidation process carried out in a liquid/solid regime, acetonitrile molecules were not able to provide a specific interaction with the surface sites of TiO_2, remaining dissolved in the interface water molecular layers. In contrast, for low H_2O/CH_3CN ratios, as is typical for the photo-oxidation process carried out in a gas–solid regime, acetonitrile could win the competition with water for surface hydroxyls.

Keywords: Acetonitrile degradation; Heterogeneous photocatalysis; TiO_2; IR investigation

1. Introduction

Among the advanced oxidation processes aimed at environmental remediation, basic and applied research has been devoted to heterogeneous photocatalysis, especially for the oxidation of organic pollutants in water or in air [1–3]. Acetonitrile is an extremely stable and toxic molecule present in various civil and industrial wastewaters; air in contact with liquid acetonitrile can be easily contaminated with acetonitrile vapour because of its low boiling temperature. It is widely used as an eluent for HPLC analyses and is commonly used in heterogeneous photocatalysis research as a solvent for molecules that are insoluble in water. Apart from its environmental hazards, acetonitrile is a very interesting molecule for use in photo-oxidation studies because it has alkyl and cyanide groups that may undergo different oxidation routes.

Lichtin and Avudaithai [4] reported the feasibility of the photocatalytic oxidation of acetonitrile in both liquid and

* Corresponding author. Fax: +39-91-6567280.
E-mail addresses: gianmario.martra@unito.it (G. Martra), palmisano@dicpm.unipa.it (L. Palmisano).

0021-9517/$ – see front matter
doi:10.1016/j.jcat.2005.08.005

vapour phases using near-UV irradiated TiO_2 Degussa P25 and O_2. They found that acetonitrile was much more reactive in the gas phase than in the liquid phase. In a gas–solid regime, they found, along with CO_2 and NO_2, cyanogen [$(CN)_2$], indicating the formation of $CN^{\cdot}$ radicals with subsequent dimerization. Zhuang et al. [5] performed FTIR investigation of acetonitrile photo-oxidation in a gas–solid system and found the oxidation products CO_2, H_2O, and CO_3^{2-} on the catalyst surface, along with isocyanate as a partially oxidized species. They did not observe hydrogen cyanide, probably because this compound was not present in adsorbed phase but was released to the gas phase. They claimed breakage of the acetonitrile C–C bond and proposed a reaction mechanism onto the catalyst surface in which the principal products are CO_2 and N_2. Augugliaro et al. [6] studied the kinetics of acetonitrile degradation in a gas–solid regime using two different continuous photoreactors to check whether the specific setup used for the reactivity experiments affected the photoprocess performance. They reported that the Langmuir–Hinshelwood model adequately described the degradation kinetics, and that the values of equilibrium adsorption constants were independent of the used photoreactor, whereas the kinetic constant values depended on the radiation conditions of the photoreactor. Sunlight has been also used for carrying out the photocatalytic oxidation of acetonitrile in aqueous suspensions of TiO_2 Degussa P25 [7]. For that system, the influence of a strong oxidant species (H_2O_2, $S_2O_8^{2-}$, ClO^-) on acetonitrile abatement was also investigated. The acetonitrile oxidation products were isocyanate and/or cyanate ions, the presence of which was a strong clue to the formation of cyanide species in the course of acetonitrile degradation.

The present paper deals with acetonitrile photodegradation carried out in both gas–solid and liquid–solid regimes using two commercial polycrystalline TiO_2 catalysts (Merck and Degussa P25). This investigation focused on studying the influence of the reaction medium (liquid or gaseous) on the kinetics and mechanisms of acetonitrile oxidation. Toward this goal, the photoreactivity experiments were planned to obtain the values of the kinetic and equilibrium adsorption constants involved in the acetonitrile degradation process. To obtain information about the reaction mechanism, the intermediate and final species appearing in the reaction environment during the photocatalytic process were identified and quantitatively determined. In addition, the competition in the dark between water and acetonitrile for TiO_2 adsorbing sites was explored by IR spectroscopy.

2. Experimental

2.1. Gas–solid regime

The reactivity runs were carried out using a continuous annular Pyrex photoreactor (Fig. 1A). The vertically positioned photoreactor was provided with inlet and outlet ports for the reacting mixture. TiO_2 Merck (100% anatase; BET specific surface area = ca. 10 $m^2\ g^{-1}$) and TiO_2 Degussa P25 (80% anatase

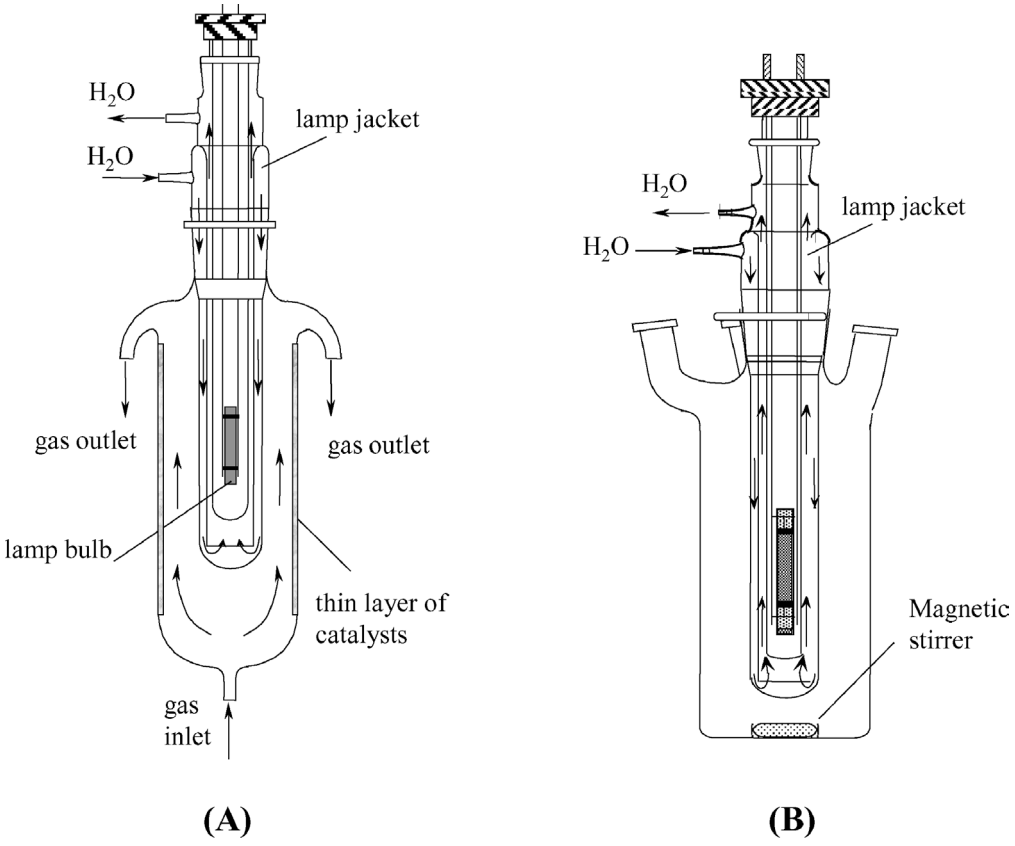

Fig. 1. Photoreactors set-up: (A) Gas–solid system; (B) liquid–solid system.

and 20% rutile; BET specific surface area = ca. 50 $m^2 g^{-1}$) were used with no preliminary treatment. A thin layer of the catalyst (1 g for both photocatalysts) covered the internal wall of the outer tube of the annulus (6.5 cm i.d., 32.0 cm tall). In these conditions, the light transmitted by the TiO_2 layer was negligible, as checked with a radiometer (UVX Digital). A 500 W medium-pressure Hg lamp (Helios Italquartz, Italy; highest emission at 365 nm), equipped with a Pyrex water-cooling thimble (5.4 cm o.d.), constituted the inner part of the annulus. The Pyrex thimble, which is completely blind to radiation with wavelength <300 nm, guaranteed that the radiation inside the photoreactor would be absorbed only by the TiO_2 catalyst.

The gas fed to the photoreactor consisted of oxygen, nitrogen, acetonitrile, and water. Liquid acetonitrile and water were added to the gas flow through an infusion pump (Orion Sage pump M 361). The concentrations used were as follows: acetonitrile, 0.1–1.1 mM; oxygen, 4–40 mM; and water vapour, 0.0–0.3 mM. A gas flow rate of 2.58 $cm^3 s^{-1}$ was used for most of the runs. The temperature of the system at steady-state conditions was 303 ± 2 K.

The run procedure was the same through the study. Irradiation was begun only after steady-state conditions were achieved in the system, that is, after about 1 h from the start of photoreactor feeding. The runs lasted 4.0 h, and the gas leaving the photoreactor was analysed periodically using an on-line gas chromatograph (Hewlett-Packard GC 6890 system) equipped with a methyl siloxane column (30 m × 320 μm × 0.25 μm; Hewlett-Packard HP-1) and an FID detector, using grade helium as a carrier. Gravimetric determination of the carbon dioxide produced was done for selected runs by bubbling the gas exiting the photoreactor in a saturated $Ba(OH)_2$ aqueous solution; the total amount of CO_2 was determined as $BaCO_3$. For each run, the gas at the outlet of the photoreactor was bubbled in an aqueous solution of NaOH (0.1 M) to trap acetonitrile degradation products. Quantitative determination of trapped cyanide ions was performed by an ion-sensitive electrode (Orion model 94-06) in an expandable ion analyser (Orion EA 920) and that of anionic species (e.g., cyanate, nitrate and methanoate) was done using an ionic chromatograph system (Dionex DX 120) equipped with an Ion Pac AS14 4-mm column (250 mm long, Dionex). Aqueous solution of $NaHCO_3$ (8 mM) and Na_2CO_3 (1 mM) were used as eluents at a flow rate of 1.67×10^{-2} $cm^3 s^{-1}$.

At the end of each run, the used catalyst was scraped from the photoreactor wall and put in water for 1 h; the resulting solution was analysed by ionic chromatography after separation of the solid by filtration through a 0.45-μm cellulose acetate filter (HA, Millipore).

The ferrioxalate actinometric method [8] was used to measure the photon flow emitted by the lamp. The used actinometric solution, which absorbs light wavelengths only in the 300–400 nm range, filled the photoreactor and was irradiated for 20 s. The measurements were repeated several times, and an average value of 7.2×10^{-5} Einstein s^{-1} was determined. All of the reagents were of analytical grade (Aldrich).

2.2. Liquid–solid regime

A cylindrical Pyrex batch photoreactor containing 1.5 L of aqueous suspension (Fig. 1B) was used for the liquid–solid regime. This photoreactor has ports in its upper section for inlet and outlet gases, for sampling, and for pH and temperature measurement. This photoreactor had the same irradiating apparatus used in the gas–solid regime, that is, a 500 W medium-pressure Hg lamp (Helios Italquartz, Italy) equipped with a Pyrex water-cooling thimble.

The same TiO_2 catalysts used in the gas–solid regime were used here as well. In all experiments, the amount of catalyst was 0.4 $g l^{-1}$. In this condition, the photon flow transmitted by the suspension was negligible for both catalysts. The initial acetonitrile concentration was varied in the range 0.24–24 mM. For some photoreactivity runs, the starting solution contained only cyanate ions, whose initial concentration varied in the range 0.45–1.45 mM. The pH of the suspension was adjusted to 11 by adding NaOH. Pure oxygen or air was continuously bubbled into the suspension before and during the runs. The temperature inside the reactor during the runs was 300 ± 2 K. The photoreactivity runs lasted 5 h; before the lamp was switched on, the system was held at the imposed operative conditions for 0.5 h. Samples (5 mL) were withdrawn at fixed time intervals for analysis. The catalyst was immediately separated from the solution by filtration through a 0.45-μm cellulose acetate filter (HA, Millipore).

The quantitative determination of CH_3CN was routinely performed with the same gas chromatograph, column, and conditions used for the gas–solid experiments following this procedure: first, 1 mL of sample was placed in a vial, and then the compounds present in the vapour phase were extracted (extraction time, 5 min) using a 75-μm carboxen-PDMS SPME (Solid Phase Micro Extraction) fibre assembly (Supelco) with a fibre holder for manual sampling. The holder was then placed in the split/splitless injector of a gas chromatograph maintained at 523 K. The oven temperature was 310 K for the first 3 min and thereafter increased to 523 K at a ramp rate of 60 K min^{-1}. The quantitative determination of ionic species was carried out as described for the gas–solid experiments. A 5000A Shimadzu total organic carbon analyser was used to determine the non-purgeable organic carbon (NPOC) content of the samples.

2.3. IR measurements

TiO_2 powder was pressed in the form of self-supporting pellets (40 mg cm^{-2}). The IR quartz cell, equipped with KBr windows, was connected to a conventional vacuum line (residual pressure = 1.00×10^{-6} Torr; 1 Torr = 133.33 Pa) allowing the performance of all adsorption–desorption experiments in situ. CD_3CN (99.8%, Aldrich) was used for the adsorption experiments instead of CH_3CN, to keep bands due to Fermi resonance from perturbing the ν(CN) mode of the probe molecule [9]. Acetonitrile and water were admitted onto the sample after several freeze–pump–thaw cycles. FTIR spectra (4 cm^{-1} resolution) were recorded with a Bruker Vector 22 spectrometer equipped with a DTGS detector.

3. Results

For both the gas–solid and liquid–solid regimes, blank tests were performed under the same experimental conditions used for the photoreactivity experiments but in the absence of catalyst, oxygen, or light. No reactivity was observed in any of these cases. The contemporary presence of O_2, catalyst, and irradiation was needed for the acetonitrile degradation process.

3.1. Photoreactivity in the gas–solid regime

Preliminary photoreactivity tests were performed at increasing flow rate values, with the aim of minimising mass transport resistances on the photocatalytic process. The reaction rate enhanced for flow rate by $\lesssim$1.1 $cm^3\,s^{-1}$, whereas for higher values it did not change significantly for either photocatalysts. These findings indicate that mass transfer resistance plays an important role for flow rates < 1.1 $cm^3\,s^{-1}$. Based on this, it was decided to carry out all of the photocatalytic experiments of acetonitrile degradation at a flow rate equal to 2.58 $cm^3\,s^{-1}$.

The acetonitrile concentrations at the inlet and outlet of the photoreactor were measured. The knowledge of these values allowed us to determine the acetonitrile disappearance rate per unit of catalyst surface area, $(-r_S)$, by applying the following mass balance on the whole photoreactor:

$$(-r_S) = \frac{W}{S}(C_{AN,I} - C_{AN,O}) \quad (1)$$

where W is the volumetric gas flow rate, S is the total surface area of catalyst, and $C_{AN,I}$ and $C_{AN,O}$ are the inlet and outlet acetonitrile molar concentrations, respectively, at steady-state conditions.

For both catalysts, Fig. 2a reports $(-r_S)$ data obtained from runs in which the inlet acetonitrile concentration was varied by keeping the inlet oxygen concentration constant. Fig. 2b reports $(-r_S)$ data obtained by varying the inlet oxygen concentration while maintaining a constant inlet acetonitrile concentration. It can be observed that the $(-r_S)$ values increased with increasing inlet acetonitrile or oxygen concentration up to an almost constant value.

For all runs, the degradation products revealed in the gas phase were carbon dioxide and hydrogen cyanide, while the ionic species found in the alkaline trap were cyanide ions and traces of methanoate ions. The moles of cyanide ions found in the alkaline trap were equal to the moles of degraded acetonitrile. Traces of nitrate and methanoate ions were found in the aqueous solution in which the used catalysts were washed at the end of the photocatalytic run.

Some runs were carried out using a dry reacting mixture. The observed values of the reaction rate were almost identical to those obtained with a wet reacting mixture. Acetonitrile degradation products were the same as those obtained with wet reacting mixtures. Both catalysts also exhibited constant activity for long runs (72 h); in these runs, the catalysts maintained their initial white colour, indicating that no coloured poisons accumulated on the irradiated surface.

3.2. Photoreactivity in the liquid–solid regime

Preliminary experiments were carried out to investigate the adsorption of acetonitrile onto the catalyst surface. Acetonitrile concentration was measured before and after the addition of TiO_2 powder to the aqueous solution. Even after long contact times (48 h), the acetonitrile concentration values were not significantly different than those of the starting solution. This indicates that acetonitrile dissolved in water scarcely adsorbs in the dark on the TiO_2 surface.

Fig. 3 reports acetonitrile concentration values versus irradiation time for runs carried out at different initial acetonitrile concentrations for both catalysts. Acetonitrile concentration decreased with increasing irradiation time, and the pattern of acetonitrile degradation was the same for both photocatalysts. No significant differences in photoreactivity resulted from bubbling air instead of oxygen (runs not reported for the sake of brevity).

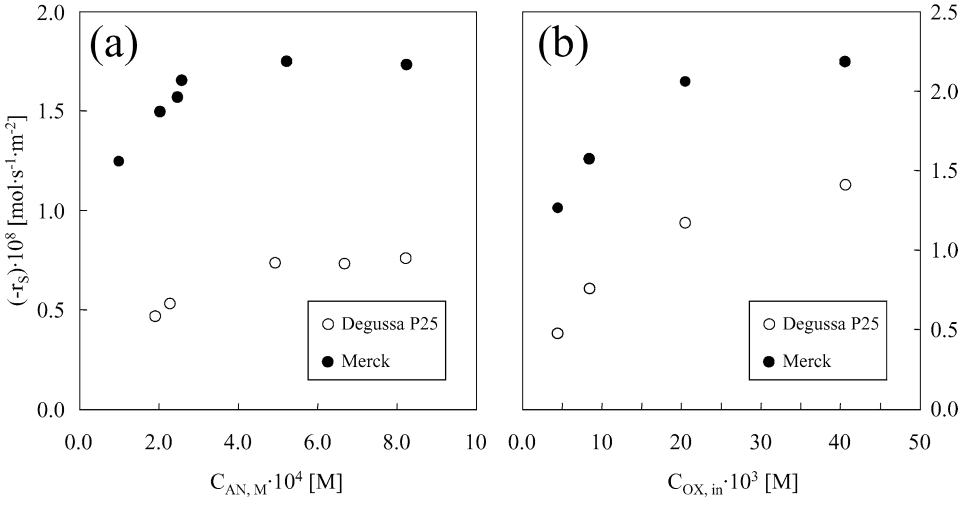

Fig. 2. (a) Specific reaction rate $(-r_S)$ versus average acetonitrile concentration for runs carried out in the gas–solid system. Oxygen initial concentration equal to 8 mM. (b) Specific reaction rate $(-r_S)$ versus inlet oxygen concentration for runs carried out in the gas–solid system. Acetonitrile initial concentration equal to 0.5 mM.

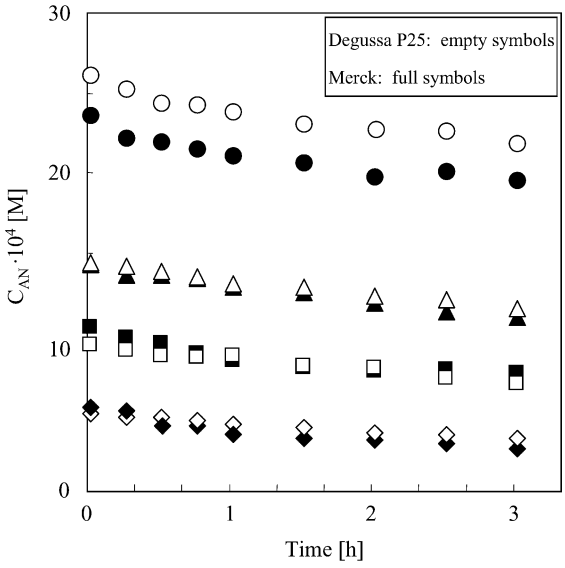

Fig. 3. Acetonitrile concentration versus irradiation time for runs carried out in the liquid–solid system.

The determination of NPOC concentration indicated that for all runs, achieving complete mineralization required more time at higher initial acetonitrile concentrations. Cyanate and carbonate ions were found in significant amounts in the aqueous solution; small amounts of cyanide, nitrite, nitrate, and methanoate ions were also detected. Both catalysts produced the same intermediate species and final products of acetonitrile degradation. Figs. 4a and b report the concentration of N-containing ionic species (cyanide, cyanate, nitrite and nitrate) and of acetonitrile versus the irradiation time for two representative runs. These figures also report the nitrogen molar balance achieved by adding the concentrations of all of the N-containing species quantitatively detected in the solution (acetonitrile, cyanide, cyanate, nitrite, and nitrate). This balance satisfied the initial nitrogen concentration for the duration of the run, indicating that volatile nitrogen compounds were not formed in the course of acetonitrile photodegradation. This behaviour was confirmed in all of the runs carried out with both catalysts.

Some runs were devoted to investigating the photodegradation kinetics of cyanate ion at the same experimental conditions used for acetonitrile degradation. As was found with acetonitrile, no significant difference of photoreactivity was observed by bubbling air or pure oxygen into the suspension. The cyanate oxidation products found in the solution were nitrate and carbonate ions; only traces of nitrite were observed, and no ammonia was detected. Fig. 5 reports cyanate concentration values versus irradiation time for runs carried out using the two catalysts at different initial cyanate concentrations.

3.3. FTIR studies

IR spectroscopic investigation of molecular events resulting from the adsorption of acetonitrile on the surface of the two TiO_2 photocatalysts and subsequent UV irradiation in model conditions has been the object of previous studies [6,10]. The results of these studies can be summarized as follows: (i) in the dark, on TiO_2 Merck, acetonitrile is adsorbed as is, whereas on TiO_2 P25, it is transformed by reaction with surface basic sites characteristic of this type of photocatalyst [11] into acetamide-like species that are highly resistant to photodegradation, and then subtract a part of the surface sites to the photocatalytic process; and (ii) the photodegradation of acetonitrile actually involves adsorbed species, likely occurring at a higher rate for molecules adsorbed on Ti^{4+} ions than those adsorbed on surface hydroxyls.

The kinetic results presented in this work, indicating that in a gas–solid regime the presence of water in the feed (up to a 3:1 molar ratio with respect to acetonitrile) does not significantly affect the photoconversion rate of acetonitrile, whereas such a rate is significantly lower in a liquid–solid regime, stimulated us to use IR spectroscopy of adsorbed species to investigate possible competition (in the absence of UV light) between acetonitrile and water molecules at the surface of TiO_2. The study was

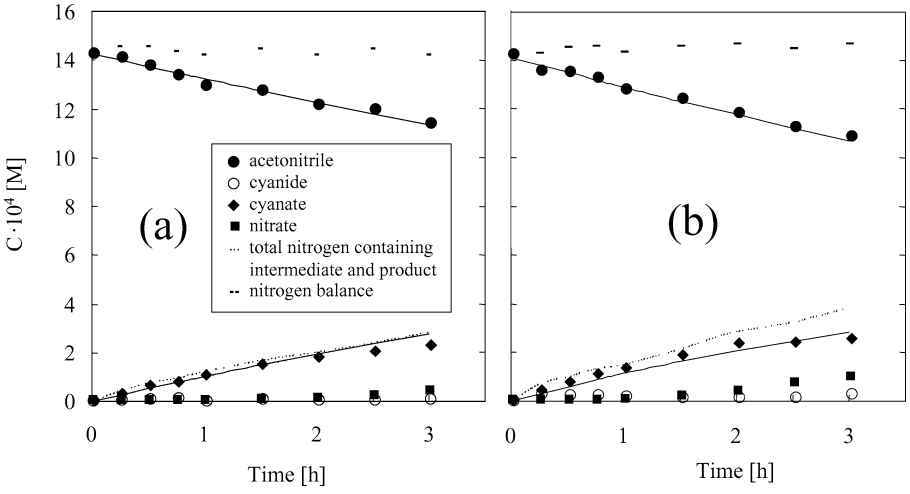

Fig. 4. Concentrations of acetonitrile, cyanide, cyanate, nitrate, total nitrogen containing intermediates and products and nitrogen balance versus irradiation time for a selected run carried out in liquid–solid system by bubbling pure oxygen. Photocatalysts: (a) TiO_2 P25 Degussa; (b) TiO_2 Merck. The lines drawn through the data represent the kinetic model [Eqs. (26) and (28)].

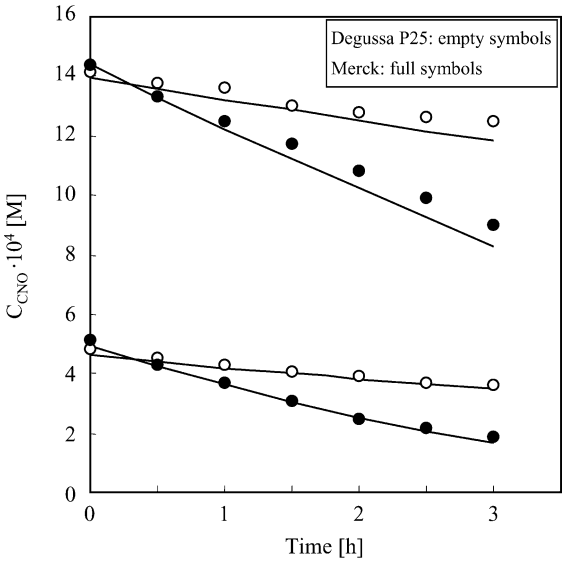

Fig. 5. Concentrations of cyanate versus irradiation time for runs carried out in liquid–solid system. The lines drawn through the data represent the kinetic model [Eq. (30)].

restrained to the TiO_2 (Merck), because acetamide-like species do not form on this photocatalyst, even in the dark.

Initially, acetonitrile alone was adsorbed on the photocatalyst outgassed simply at room temperature. In this condition the TiO_2 surface is still completely covered with a full monolayer of hydroxyl groups and coordinated water molecules, as should occur in the first interface layer at both the solid–gas and the solid–liquid boundaries in the photocatalytic runs.

The spectrum of the TiO_2 outgassed at room temperature exhibited a peak at 3665 cm^{-1} (Fig. 6a), a very broad band in the 3500–3000 cm^{-1} range, a complex band centred at 1640 cm^{-1}, and some other weak components at lower frequencies. The peak at higher wave numbers can be assigned to the stretching mode of isolated hydroxyl groups, whereas the broad band in the 3500–3000 cm^{-1} range should result from the overlap of the bands due to the stretching mode of hydrogen-bonded –OH groups and of water molecules coordinated with Ti^{4+} ions, the bending mode of which produces the component at 1640 cm^{-1} of the complex signal in the 1750–1550 cm^{-1} range (Fig. 6, inset A, graph a) [12–14]. The other components in the 1750–1300 cm^{-1} range are due to carbonate-like groups, produced by reaction by CO_2 with surface basic centres during the storage of photocatalyst powder in air.

Increasing doses of CD_3CN produce a progressive decrease in intensity of the peak at 3665 cm^{-1}, with transformation into a broad absorption in the 3500–3000 cm^{-1} range (Figs. 6b–d). This behaviour clearly indicates that the isolated hydroxyl groups act as adsorption sites for acetonitrile, with the observed downshift of their stretching band resulting from the interaction between such OH groups and lone pairs on the N atoms of CD_3CN. The adsorption of acetonitrile was stopped after disappearance of the 3665 cm^{-1} peak due to unperturbed OH groups, to avoid the formation of CD_3CN liquid-like overlayers. At lower frequencies, the component at 1640 cm^{-1} appeared eroded to a slight extent (Fig. 6, inset A), indicating that part of the water molecules coordinated to surface cations had been displaced by acetonitrile, passing in the vapour phase. The same behaviour was observed for the adsorption of acetonitrile on TiO_2 P25 [10], although here it was more evident because of the greater number of water molecules on such types of titania [11].

Peaks due to adsorbed acetonitrile appeared in the 2350–2100 cm^{-1} range, observed more clearly in the zoomed difference spectra reported in inset B of Fig. 6. The main peak at

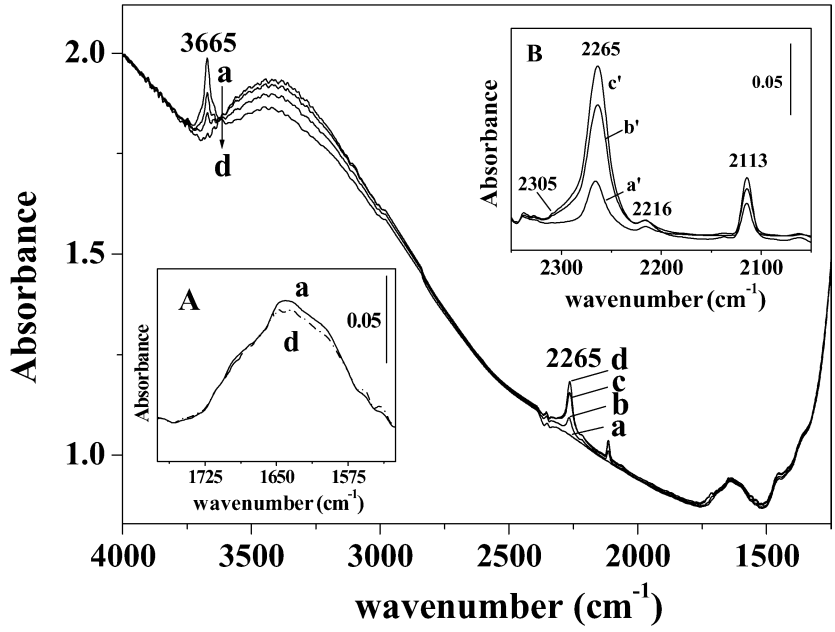

Fig. 6. IR spectra of TiO_2 Merck: (a) outgassed at room temperature for 45 min and then contacted with (b) 0.3, (c) 0.7, and (d) 1.0 Torr CD_3CN. An enlarged view of spectra (a) and (d) in the 1775–1525 cm^{-1} range is reported in the inset A. Inset B: spectra, in the 2330–2050 cm^{-1} range, of adsorbed CD_3CN obtained by subtracting spectrum (a)—TiO_2 before CD_3CN admission—from spectra (b), (c), (d); the results are indicated as: (a′) 0.3, (b′) 0.7, and (c′) 1.0 Torr CD_3CN.

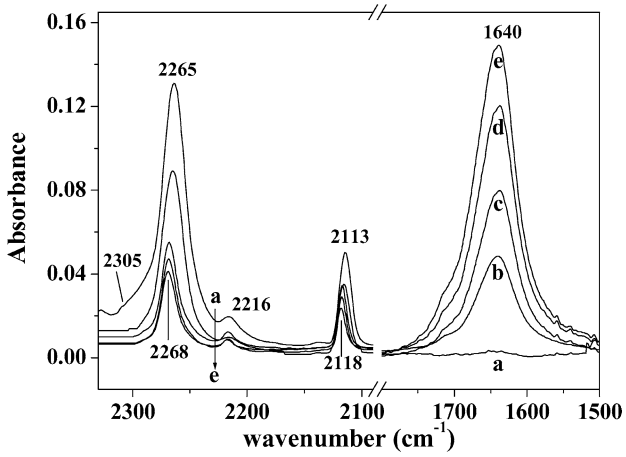

Fig. 7. IR spectra recorded after admission of increasing doses of water vapour on TiO_2 Merck with preadsorbed CD_3CN: (a) CD_3CN alone (1.0 Torr), the same as curve c′ in the inset of Fig. 6; after admission of water vapour to reach the following pressure in the cell: (b) 2.0, (c) 5, (d) 10, and (e) 18 Torr. The spectra are reported in Absorbance, after subtraction of the spectrum of the TiO_2 pellet initially outgassed at room temperature prior CD_3CN adsorption.

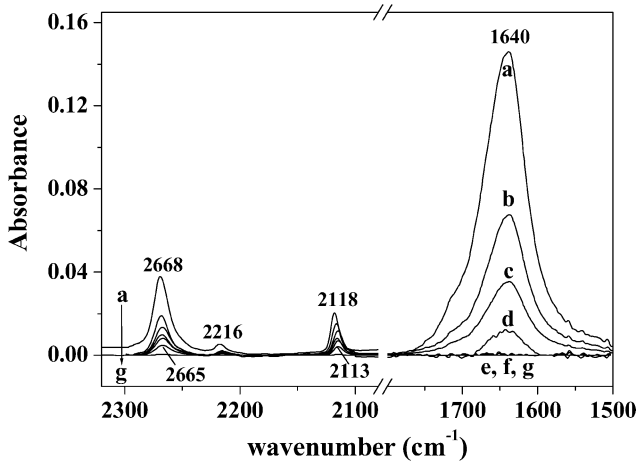

Fig. 8. IR spectra recorded at decreasing coverage of co-adsorbed CD_3CN and H_2O: (a) 18 Torr (the same as curve e in Fig. 7), (b) 4.0, (c) 2.0, (d) 1.0 Torr, (e–g) upon outgassing for increasing time, up to 10 min. The spectra are reported in Absorbance, after subtraction of the spectrum of the TiO_2 pellet initially outgassed at room temperature prior CD_3CN and water adsorption.

2265 cm^{-1} and its shoulder at 2305 cm^{-1} are due to ν(CN) mode of CD_3CN molecules adsorbed on hydroxyls groups and Ti^{4+} sites, respectively [10]. The upward shift of these components with respect to the ν(CN) mode of liquid CD_3CN (2262 cm^{-1}) [15] results from interaction with the adsorbing centres, becoming larger with increasing Lewis acid strength of the sites [15].

Furthermore, the weaker absorptions at 2216 and 2113 cm^{-1} correspond to the $2\nu(CC) + \delta_{asym}(C–C{\equiv}N)$ combination band and the $\nu_{sym}(CD_3)$ mode, respectively [16]. Apparently, both of these are less sensitive to the Lewis acidity of the adsorbing sites.

As a second step, increasing amounts of water vapour were admitted on the sample with preadsorbed acetonitrile in the presence of water vapour pressure at room temperature (total pressure, ca. 18 Torr). The increasing adsorption of H_2O molecules on the photocatalyst surface resulted in the formation of molecular "liquid-like" adlayers producing the growth of a band at 1640 cm^{-1} in the IR spectra due to the δ_{H_2O} mode, as well as modifications of the bands related to adsorbed CD_3CN (Fig. 7). In particular, the shoulder at 2305 cm^{-1} disappeared after the admission of the first doses (Figs. 7a and b), reflecting the displacement of CD_3CN molecules from Ti^{4+} ions, whereas the bands related to CD_3CN initially adsorbed on hydroxyl groups exhibited a decrease in intensity and a shift toward higher frequencies (more pronounced for the two peaks initially at 2265 and 2113 cm^{-1}, due to fundamental vibrations of CD_3CN) as the amount of adsorbed water increased (Figs. 7a–e). Notably, the final position and ratio of intensity of these components corresponded to those of the IR spectrum of CD_3CN dissolved in water (not reported for the sake of brevity).

A subsequent progressive outgassing of the system resulted in desorption of co-adsorbed acetonitrile and water molecules in the IR spectra from a decreased intensity of the δ_{H_2O} band at 1640 cm^{-1} and of the spectral pattern due to CD_3CN in the 2300–2100 cm^{-1} range (Fig. 8). Two important features related to the CD_3CN bands merit mention: (i) they shifted progressively toward the original positions that they exhibited when in interaction with surface hydroxyl groups; and (ii) they decreased in intensity less markedly with respect to the δ_{H_2O} band under progressive outgassing, still present after this last band vanished (Figs. 8e, f). They finally disappeared (Fig. 8g), due to full reversibility of the interaction with the hydroxyl groups at room temperature, as observed in previous investigations [10].

4. Discussion

4.1. Mechanistic aspects

In the gas–solid regime, CO_2 and HCN were the main products of acetonitrile degradation for both photocatalysts. The HCN formation revealed by gas chromatography was confirmed by analysis of the alkaline solution contained in the trap. The moles of cyanide ions corresponded to those of degraded acetonitrile. The second carbon atom present in the acetonitrile molecule was almost quantitatively transformed into CO_2, as determined by the gravimetric method. These findings support the hypothesis of Zhuang et al. [5] claiming breakage of the acetonitrile C–C bond. The presence of traces of methanoate ions in the trap can be attributed to the partial oxidation of the organic moiety of the molecule. Moreover, it is noteworthy that the very small quantities of methanoate ions along with nitrate ions found adsorbed on the surface of the used catalysts confirm that acetonitrile was transformed almost completely to HCN and CO_2. The production of CO_2 and HCN from acetonitrile degradation in the gas–solid regime can be described by the following overall reaction:

$$CH_3CN + \tfrac{3}{2}O_2 \xrightarrow[h\nu]{TiO_2} CO_2 + HCN + H_2O. \quad (2)$$

In the liquid–solid regime, the acetonitrile photodegradation process produced cyanate and carbonate ions and very small amounts of cyanide, nitrite, nitrate, and methanoate ions. Based

on this finding, it may be assumed that the catalyst irradiation for both regimes determines the acetonitrile photoadsorption [5,17–20] on TiO_2 surface sites. Lichtin and Avudaithai [4] hypothesized that the reaction between adsorbed acetonitrile and phototoproduced $^{\cdot}OH$ radicals is able to perform C–C bond breakage with the production of cyanide radicals and methanol:

$$TiO_2 \xrightarrow{h\nu} TiO_2(h^+, e^-), \tag{3}$$

$$O_2 + e^- \rightarrow {}^{\cdot}O_2{}^-, \tag{4}$$

$${}^{\cdot}O_2{}^- + H_2O \rightarrow HO_2{}^{\cdot} + OH^-, \tag{5}$$

$$OH^- + h^+ \rightarrow {}^{\cdot}OH, \tag{6}$$

$$CH_3CN_{(ads)} + {}^{\cdot}OH \rightarrow CH_3OH + CN^{\cdot}. \tag{7}$$

In the gas–solid regime, the $CN^{\cdot}$ radicals reacted with water adsorbed on the catalyst surface, giving rise to the formation of HCN, whereas methanol was photo-oxidised to CO_2:

$$CN^{\cdot} + H_2O \rightarrow HCN + {}^{\cdot}OH, \tag{8}$$

$$CH_3OH + 6{}^{\cdot}OH \rightarrow CO_2 + 5H_2O. \tag{9}$$

In contrast, in the liquid–solid regime, most of the cyanide radicals were transformed into cyanate ions, which desorbed from the surface to the aqueous solution. The remaining cyanide radicals produced cyanide ions, which were also released to the solution:

$$CN + 2OH^- + h^+ \rightarrow CNO^- + H_2O, \tag{10}$$

$$CN^{\cdot} + OH^- \rightarrow CN^- + {}^{\cdot}OH. \tag{11}$$

The cyanide ions produced through reaction (11) underwent photocatalytic oxidation to cyanate [10,21–23]. The process continued with cyanate photo-oxidation steps, giving rise to the formation of carbonate and nitrate ions:

$$CNO^- + 10OH^- + 8h^+ \rightarrow {CO_3}^{2-} + {NO_3}^- + 5H_2O. \tag{12}$$

Methanol (species not detected, probably due to its fast oxidation), formed according to (7), was oxidised to methanale, methanoate, and carbonate ions, although only the last two species were detected:

$$CH_3OH + 2{}^{\cdot}OH \rightarrow HCOH + 2H_2O, \tag{13}$$

$$HCOH + 3OH^- + 2h^+ \rightarrow HCOO^- + 2H_2O, \tag{14}$$

$$HCOO^- + 3OH^- + 2h^+ \rightarrow {CO_3}^{2-} + 2H_2O. \tag{15}$$

In conclusion, acetonitrile photodegradation led to the formation of cyanate ions from the nitrile group and to their subsequent oxidation to nitrate and carbonate ions [reaction (12)], whereas methanol gave rise to carbonate ion as the final product [reactions (13)–(15)].

4.2. IR data: acetonitrile/water competition

The spectral features observed by admitting water vapour on the photocatalyst with preadsorbed acetonitrile (Figs. 6 and 7) indicated that nitrile molecules initially adsorbed on hydroxyl groups were converted in a solute in the molecular water layers formed at the TiO_2 surface. This condition can be assumed as a model of the photocatalyst–solution interface in the liquid–solid regime, where no specific interactions between acetonitrile molecules and the TiO_2 surface should occur because of competition with the prevailing amount of water molecules. This fact agrees well with the strong decrease in the rate constant of acetonitrile photo-oxidation resulting from passage from the gas–solid regime to the liquid–solid regime.

As for the results obtained by progressively decreasing the total amount of adsorbed molecules to a monolayer or less (Figs. 8), acetonitrile molecules were able to interact with surface hydroxyl groups slightly more strongly than water molecules. Indeed, a slightly higher interaction energy of 5 kJ mol^{-1} in favour of acetonitrile with respect to H_2O was obtained in the modeling of their adsorption on silanols [24,25]. This finding can be related to the kinetic analysis of the acetonitrile conversion in the gas–solid regime, and it is evident that the presence of small amount of water in the reaction feed did not alter the rate constant with respect to that obtained for a dry feed. Apparently, in these conditions the weak energetic advantage in the adsorption of acetonitrile with respect to water makes the competition of this latter less effective toward acetonitrile for the surface sites.

4.3. Kinetic aspects

To model the photoreactivity results obtained in the gas–solid and liquid–solid regimes, the assumption is made that all of the elementary reactions of acetonitrile degradation occur on the catalyst surface and involve adsorbed species. The rate-determining step of the photo-oxidation process is hypothesized to be the reaction on the photocatalyst surface between hydroxyl radicals and adsorbed acetonitrile molecules. The catalyst surface has sites able to adsorb acetonitrile together with its degradation products, as well as sites able to adsorb oxygen. Because the adsorbed oxygen acts as an electron trap, hindering the electron hole recombination, the $^{\cdot}OH$ concentration depends on the fractional site coverage by oxygen molecules. In this hypothesis, the acetonitrile degradation rate per unit surface area, $(-r_S)$, for a second-order kinetic may be written in terms of Langmuir–Hinshelwood model as

$$(-r_S) \equiv -\frac{1}{S}\frac{dN_{AN}}{dt} = k''_{AN}\theta_{Ox}\theta_{AN}, \tag{16}$$

where S is the surface area of the photocatalysts, N_{AN} is the acetonitrile moles, t is the time, k''_{AN} is the surface second-order rate constant, and θ_{Ox} and θ_{AN} are the fractional site coverages by oxygen and acetonitrile, respectively. The θ_{Ox} and θ_{AN} terms are given by

$$\theta_{Ox} = \frac{K_{Ox}C_{Ox}}{1 + K_{Ox}C_{Ox}} \quad \text{and} \tag{17}$$

$$\theta_{AN} = \frac{K_{AN}C_{AN}}{1 + K_{AN}C_{AN} + \sum K_I C_I}, \tag{18}$$

in which K_{Ox}, K_{AN}, and K_I are the equilibrium adsorption constants of oxygen, acetonitrile, and intermediate products, respectively, and C_{Ox}, C_{AN}, and C_I are the oxygen, acetonitrile,

and intermediate product concentrations in the fluid phase, respectively.

4.3.1. Gas–solid regime

The reactivity results show that acetonitrile is completely converted to equimolar amounts of HCN and CO_2, which were the unique species found in the gas phase. In this system, the concentration of intermediate products, C_I, in the gas phase was negligible, and thus it may be assumed that they do not compete with acetonitrile for adsorption on the catalyst surface. By putting $C_I = 0$ in (18) and substituting (17) and (18) in (16), the acetonitrile degradation rate is

$$(-r_S) = k''_{AN}\left(\frac{K_{Ox}C_{Ox}}{1+K_{Ox}C_{Ox}}\right)\left(\frac{K_{AN}C_{AN}}{1+K_{AN}C_{AN}}\right). \quad (19)$$

The photoreactivity runs exhibited a high conversion of acetonitrile, so that the assumption of a differential photoreactor is not valid. An acetonitrile molar balance on a differential control volume of the reactor may be written as

$$-W\,dC_{AN} = (-r_S)\,dS, \quad (20)$$

where dS is the surface area of the photocatalyst in the control volume.

Considering that the oxidation of one mole of acetonitrile requires only 1.5 mol of oxygen [Eq. (2)] and that the oxygen concentration at the inlet of photoreactor was at least one order of magnitude higher than that of acetonitrile under the experimental conditions here, it can be assumed that the oxygen concentration from the inlet to the outlet of the photoreactor did not change substantially. Consequently, the oxygen coverage on the catalyst also did not vary substantially from the inlet to the outlet. Based on this assumption, substituting (19) into (20) leads to the following differential mass balance on acetonitrile:

$$-W\,dC_{AN} = k'_{AN}\left(\frac{K_{AN}C_{AN}}{1+K_{AN}C_{AN}}\right)dS, \quad (21)$$

where

$$k'_{AN} = k''_{AN}\left(\frac{K_{Ox}C_{Ox,M}}{1+K_{Ox}C_{Ox,M}}\right) \quad (22)$$

is a term constant for each run. In (22), $C_{Ox,M}$ indicates the oxygen concentration value averaged between the inlet and outlet of the photoreactor; this term is introduced to take into account the small variation of oxygen concentration along the photoreactor. The integration of (21), with the limit conditions that at $S = 0$ (the inlet of photoreactor) $C_{AN} = C_{AN,I}$ and at $S = S$ (the outlet of photoreactor) $C_{AN} = C_{AN,O}$, gives, after rearrangement,

$$\ln\frac{C_{AN,I}}{C_{AN,O}} = \frac{K_{AN}}{W}k'_{AN}S - K_{AN}(C_{AN,I}-C_{AN,O}). \quad (23)$$

Eq. (23) represents a straight line in a $\ln(C_{AN,I}/C_{AN,O})$ versus $(C_{AN,I} - C_{AN,O})$ coordinate system; the experimental data are reported in Fig. 9 using the previous coordinates. Using a least squares best-fitting procedure, straight lines were fit through the data, and the values of K_{AN} and k'_{AN} were determined. The values of k'_{AN} depend on oxygen concentration by following (22);

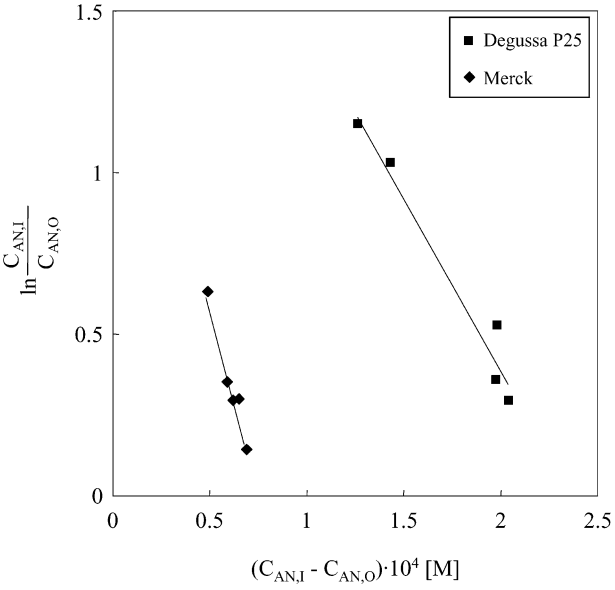

Fig. 9. Experimental data of $\ln(C_{AN,I}/C_{AN,O})$ versus $(C_{AN,I} - C_{AN,O})$. The straight lines drawn through the data represent the kinetic model [Eq. (23)].

Table 1
Values of rate constant for acetonitrile (k''_{AN}) and cyanate (k''_{CNO}) disappearance and of equilibrium adsorption constants of acetonitrile (K_{AN}), cyanate (K_{CNO}), and oxygen (K_{Ox}) according to the Langmuir–Hinshelwood kinetic model. The A constant is equal to ($k''_{CNO}K_{CNO}/k''_{AN}K_{AN}$)

	Merck		Degussa P25	
	Gas–solid	Liquid–solid	Gas–solid	Liquid–solid
k''_{AN} (mol s^{-1} m^{-2})	3.01×10^{-8}	1.11×10^{-8}	2.11×10^{-8}	2.02×10^{-9}
k''_{CNO} (mol s^{-1} m^{-2})	–	2.08×10^{-8}	–	1.60×10^{-9}
K_{AN} (M^{-1})	23,060	2600	10,640	1900
K_{CNO} (M^{-1})	–	1900	–	1200
K_{Ox} (M^{-1})	240	–	90	–
A	–	1.37	–	0.50

this equation can be transformed to a linear equation in the following way:

$$\frac{1}{k'_{AN}} = \frac{1}{k''_{AN}K_{Ox}}\frac{1}{C_{Ox,M}} + \frac{1}{k''_{AN}}. \quad (24)$$

Eq. (24) represents a straight line in a $1/k'_{AN}$ versus $1/C_{Ox,M}$ coordinate system. Using the usual fitting procedure, the values of k''_{AN} and K_{Ox} were obtained. The values of k''_{AN} and of K_{AN} and K_{Ox}, reported in Table 1, indicate that TiO_2 Merck has better photocatalytic performance than TiO_2 Degussa P25.

4.3.2. Liquid–solid regime

As discussed earlier, the disappearance of acetonitrile in the liquid–solid regime occurs through the same pathway as in the gas–solid regime and involves sites that are able to break the C–C bond. This route transforms acetonitrile in cyanide, cyanate, nitrate, and carbonate ions. The finding that in aqueous solution, cyanate concentration is far higher than cyanide ion concentration after the start of acetonitrile photodegradation indicates that the cyanide radicals, photoproduced on the catalyst surface, are transformed predominantly to cyanate instead

of cyanide ions. Based on this finding, we make the assumption that the parallel route producing cyanide ions can be neglected for the kinetic modeling of acetonitrile photodegradation.

It is useful to keep in mind that all of the photoreactivity runs in the liquid–solid regime with either acetonitrile or cyanate ion were carried out in a batch reactor by continuously bubbling oxygen or air into the reacting suspension. Consequently, the fractional site coverage by oxygen, θ_{Ox}, remained constant throughout the photoreactivity run. Moreover, for both catalysts, no significant difference in photoreactivity toward acetonitrile or cyanate ion was observed by bubbling pure oxygen or air. This finding indicates that under the experimental conditions, the fractional site coverage by oxygen was equal to unity for all of the reactivity runs, that is, $\theta_{Ox} = 1$.

For modeling the photoreactivity results, it is useful to express the kinetic law as a function of the concentration of dissolved acetonitrile, C_{AN}, because it was the parameter measured experimentally. Introducing the reaction volume, V, in the definition of the reaction rate [see (16)] and the unit value of θ_{Ox}, the kinetics of acetonitrile disappearance are expressed as

$$(-r_S) \equiv -\frac{1}{S}\frac{dN_{AN}}{dt} = -\frac{V}{S}\frac{dC_{AN}}{dt} = k''_{AN}\theta_{AN}. \tag{25}$$

As far as the θ_{AN} term is concerned, the intermediate product of acetonitrile degradation is cyanate ion, which may be photocatalytically transformed to nitrate ion. Based on this finding, in (18) the $\sum K_I C_I$ term is equal to $K_{CNO}C_{CNO}$, where K_{CNO} is the equilibrium adsorption constant and C_{CNO} is the concentration of cyanate ion. Therefore, the disappearance rate of acetonitrile is

$$-\frac{V}{S}\frac{dC_{AN}}{dt} = k''_{AN}\frac{K_{AN}C_{AN}}{1 + K_{AN}C_{AN} + K_{CNO}C_{CNO}}. \tag{26}$$

Solving (26) requires determining the dependence of cyanate concentration on irradiation time, that is, modeling the kinetics of cyanate photo-oxidation. The assumption is made that the second-order kinetic model used for acetonitrile degradation also holds for cyanate photodegradation; that is, the cyanate degradation rate per unit surface area, $-r_{CNO}$, depends on the cyanate and oxygen fractional coverages. Considering that cyanate ion is produced in the first step of acetonitrile degradation but is consumed by its subsequent oxidation to nitrate ion, the rate of cyanate formation in the course of acetonitrile degradation is given by the following equation:

$$\begin{aligned} r_{CNO} &\equiv \frac{1}{S}\frac{dN_{CNO}}{dt} = \frac{V}{S}\frac{dC_{CNO}}{dt} \\ &= k''_{AN}\theta_{AN}\theta_{Ox} - k''_{CNO}\theta_{CNO}\theta_{Ox}, \end{aligned} \tag{27}$$

in which k''_{CNO} and θ_{CNO} are the second-order rate constant and fractional site coverage of cyanate ion, respectively. Taking into account that the value of θ_{Ox} is 1, substitution of the explicit expressions of θ_{AN} and θ_{CNO} in (27) yields

$$\frac{V}{S}\frac{dC_{CNO}}{dt} = \frac{k''_{AN}K_{AN}C_{AN} - k''_{CNO}K_{CNO}C_{CNO}}{1 + K_{AN}C_{AN} + K_{CNO}C_{CNO}}. \tag{28}$$

The differential Eqs. (26) and (28) are coupled, so they must be solved simultaneously. These equations contain four unknown parameters: k''_{AN}, k''_{CNO}, K_{AN}, and K_{CNO}. The values of k''_{CNO} and K_{CNO} may be determined by reactivity runs carried out with suspensions containing only cyanate ions (see Fig. 5). Assuming that the kinetic model, adopted in the presence of acetonitrile, is also valid for cyanate ion alone, the disappearance rate of cyanate ions may be expressed by the following equation:

$$-\frac{V}{S}\frac{dC_{CNO}}{dt} = k''_{CNO}\theta_{CNO}\theta_{Ox} = k''_{CNO}\frac{K_{CNO}C_{CNO}}{1 + K_{CNO}C_{CNO}}, \tag{29}$$

where the θ_{Ox} value of 1 has been substituted. Eq. (29) can be easily integrated, with the limiting condition that at the start of irradiation, $t = 0$, the cyanate ion concentration is the initial one, $C_{CNO} = C_{CNO,0}$. Thus the following integral relationship between C_{CNO} and t is obtained:

$$t = \frac{V}{S}\frac{1}{k''_{CNO}K_{CNO}}\ln\left(\frac{C_{CNO,0}}{C_{CNO}}\right) + \frac{V}{S}\frac{1}{k''_{CNO}}(C_{CNO,0} - C_{CNO}). \tag{30}$$

The values of k''_{CNO} and K_{CNO} were obtained by applying a least squares best-fitting procedure to the experimental values of C_{CNO} versus t; these are reported in Table 1. In Fig. 5, the lines drawn through the data represent (30) in which the previous values of k''_{CNO} and K_{CNO} have been substituted; a very good fit of the kinetic model to the data can be seen.

To determine the values of k''_{AN} and K_{AN}, the ratio between (28) and (26) was calculated, giving rise to the following equation:

$$-\frac{dC_{CNO}}{dC_{AN}} = 1 - \frac{k''_{CNO}K_{CNO}}{k''_{AN}K_{AN}}\frac{C_{CNO}}{C_{AN}} = 1 - A\frac{C_{CNO}}{C_{AN}}, \tag{31}$$

which contains only one unknown parameter, the A constant (equal to $k''_{CNO}K_{CNO}/k''_{AN}K_{AN}$). Integrating (31) with the limit condition that $C_{CNO} = 0$ for $C_{AN} = C_{AN,0}$ gives

$$C_{CNO} = \frac{C_{AN,0}^{1-A}C_{AN}^{A} - C_{AN}}{1 - A}. \tag{32}$$

For each catalyst, the value of A satisfying all of the reactivity runs was determined by a least squares best-fitting procedure; these values are reported in Table 1. Fig. 10 reports the experimental values of C_{CNO} versus C_{AN} for some representative runs of each catalyst; the lines drawn through the data represent the model equation (32) and indicate a very good fit of the kinetic model to the experimental data.

The integration of (26) and (28) was done by the Runge–Kutta method using the nonlinear fit protocol of Mathematica 4.1 software. The two differential equations contain an unknown parameter, k''_{AN} or K_{AN}. The value of this parameter that best fits the kinetic model to the experimental values was determined using an iterative procedure. Table 1 reports the values of k''_{AN} and K_{AN} obtained with this procedure for both catalysts. The full lines drawn through the data in Fig. 4 represent the kinetic model [(26) and (28)]. A very good fit of the experimental data to the model can be seen, indicating that the kinetic model describes the photoreactivity results well.

Examining the parameters relative to acetonitrile photodegradation reported in Table 1 shows that the values for Merck

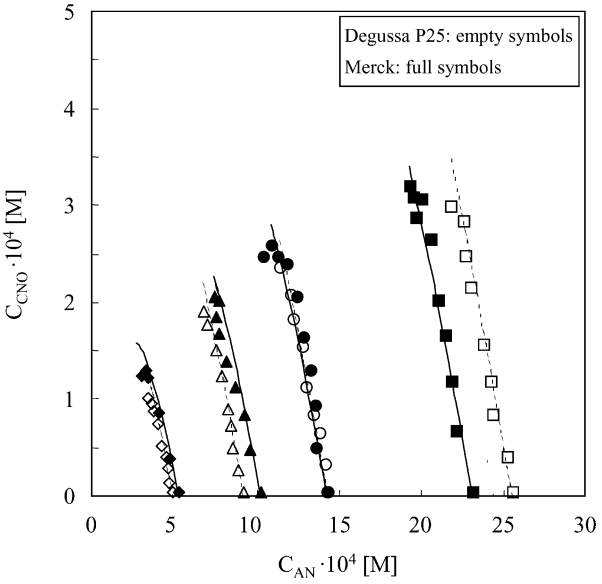

Fig. 10. Cyanate concentration versus acetonitrile concentration for runs carried out in liquid–solid system. The lines drawn through the data (dotted line Degussa P25, continuous line Merck) represent the kinetic model [Eq. (32)].

TiO_2 were always higher than those for Degussa P25 TiO_2. The photoprocess performance in both the liquid–solid and gas–solid regimes was higher with Merck TiO_2 than with P25 TiO_2. The presence of liquid water negatively affected the kinetic constant values with respect to those obtained in the gas phase; for the P25 catalyst, the k''_{AN} value decreased by about one order of magnitude, whereas the decrease for Merck was only threefold. The liquid water also negatively affects the equilibrium adsorption constant of acetonitrile; both catalysts showed significantly lower K_{AN} values; this effect was more important for Merck TiO_2 than for P25 TiO_2. In the gas–solid regime, the equilibrium adsorption constant of acetonitrile was two orders of magnitude higher than that of oxygen for both catalysts. This finding obviously indicates that photoadsorption is easier for a vapour than for a gas. The kinetic constant and equilibrium adsorption constant of cyanate photodegradation were similar to those of acetonitrile photodegradation. The k''_{CNO} value for Merck TiO_2 was more than one order of magnitude higher than that for Degussa P25 TiO_2, whereas the K_{CNO} value was a little higher in the former than in the latter.

Although making a straightforward correlation between the kinetic parameters and adsorption properties of a species is generally very difficult (because the surface sites in heterogeneous photocatalysis are produced under irradiation), it can be envisaged that the liquid medium hinders both the adsorption and the photoreactivity of dissolved molecules.

5. Conclusions

The photoreactivity results indicate that photocatalytic degradation of acetonitrile occurred in the gas–solid and liquid–solid regimes using commercial TiO_2 catalysts (Degussa P25 and Merck). The intermediate products cyanide, cyanate, nitrate, carbonate, and methanoate ions were found in the liquid–solid regime, whereas hydrogen cyanide and CO_2 were found in the gas–solid regime. These findings suggest breakage of the acetonitrile C–C bond in both regimes. In the gas–solid regime, nitrile moiety formed a cyanide radical that evolved to volatile hydrogen cyanide, whereas the methyl moiety underwent a fast and quantitative oxidation to CO_2 and H_2O. In the liquid–solid regime, the acetonitrile molecule follows the same route of degradation as seen in the gas–solid regime, characterised by C–C breaking. The nitrile part of the acetonitrile molecule formed cyanate, which was released to the aqueous solution for subsequent photocatalytic oxidation to nitrate and carbonate, whereas oxidation of the methyl moiety was relatively slow, allowing the detection of a certain quantity of methanoate.

Photocatalytic degradation kinetics in both regimes can be described using the Langmuir–Hinshelwood model. A comparison between the constants obtained by kinetic modeling indicates that liquid water played a fundamental role in the photoprocess performance. In fact, the liquid medium hindered both the adsorption and the photoreactivity of dissolved molecules. As for the adsorption in the dark, IR data confirmed the role of water as the predominant competitor for TiO_2 surface sites with respect to acetonitrile molecules, which in turn interacted preferentially with the TiO_2 surface when the acetonitrile–water gaseous feed is poor in water.

Acknowledgments

The authors thank MIUR for financial support (PRIN projects 2003035534_00X and 2003035534_004).

References

[1] M. Schiavello (Ed.), Heterogeneous Photocatalysis, Wiley, New York, 1995.
[2] M.R. Hoffmann, T.S. Martin, W. Choi, D.W. Bahnemann, Chem. Rev. 95 (1995) 69.
[3] A. Fujishima, K. Hashimoto, T. Watanabe, TiO_2 Photocatalysis: Fundamentals and Applications, Bkc, Tokyo, 1999.
[4] N.N. Lichtin, M. Avudaithai, Environ. Sci. Technol. 6 (1996) 2014.
[5] J. Zhuang, C.N. Rusu, J.T. Yates Jr., J. Phys. Chem. B 103 (1999) 6957.
[6] V. Augugliaro, S. Coluccia, E. García-López, V. Loddo, G. Marcì, G. Martra, L. Palmisano, M. Schiavello, Top. Catal. 2005, in press.
[7] V. Augugliaro, A. Bianco Prevot, J. Cáceres Vázquez, E. García-López, A. Irico, V. Loddo, S. Malato Rodríguez, G. Marcì, L. Palmisano, E. Pramauro, Adv. Environ. Res. 8 (2004) 329.
[8] S.L. Murov (Ed.), Handbook of Photochemistry, Dekker, New York, 1973.
[9] H. Knözinger, H. Krietenbrink, J. Chem. Soc., Faraday Trans. 91 (1975) 2421.
[10] P. Davit, G. Martra, S. Coluccia, V. Augugliaro, E. García-López, V. Loddo, G. Marcì, L. Palmisano, M. Schiavello, J. Mol. Catal. A: Chem. 204–205 (2003) 693.
[11] G. Martra, Appl. Catal. A: Gen. 200 (2000) 275.
[12] G. Munuera, F.S. Stone, Discuss. Faraday Soc. 52 (1971) 205.
[13] D.M. Griffiths, C.H. Rochester, J. Chem. Soc., Faraday Trans. 1 73 (1977).
[14] C. Morterra, J. Chem. Soc., Faraday Trans. 1 84 (1986) 1617.
[15] E. Escalona Platero, M. Peñarroya Mentruit, C. Morterra, Langmuir 15 (1999) 5079, and reference therein.
[16] C. Binet, A. Jadi, J.C. Lavalley, J. Chem. Phys. 89 (1992) 31.
[17] J. Cunningham, M. Jauch, D. McNamara, Proc. R. Ir. Acad. 89 (1989) 299.
[18] K. Hadjiivanov, D. Klissurski, G. Busca, V. Lorenzelli, J. Chem. Soc., Faraday Trans. 87 (1991) 175.

[19] R.I. Bickley, in: M. Schiavello (Ed.), Heterogeneous Photocatalysis, Wiley, New York, 1995.
[20] J. Cunningham, P. Sedlak, Catal. Today 29 (1996) 309.
[21] J. Peral, X. Domenech, J. Photochem. Photobiol. A: Chem. 53 (1992) 93.
[22] V. Augugliaro, V. Loddo, M.J. López-Muñoz, G. Marcì, L. Palmisano, J. Catal. 166 (1997) 272.
[23] V. Augugliaro, J. Blanco Gálvez, J. Cáceres Vázquez, E. García López, V. Loddo, M.J. López-Muñoz, S. Malato, G. Marcì, L. Palmisano, M. Schiavello, J. Soria, Catal. Today 54 (1999) 45.
[24] A.G. Pelmenshikov, G. Morosi, A. Gamba, J. Phys. Chem. 96 (1992) 7422.
[25] A.G. Pelmenshikov, G. Morosi, A. Gamba, S. Coluccia, J. Phys. Chem. 99 (1995) 15018.